



Article

Analysis of Soot Deposition Mechanisms on Nickel-Based Anodes of SOFCs in Single-Cell and Stack Environment

Konrad Motylinski ^{1,2,3,*}, Marcin Blesznowski ^{1,2}, Marek Skrzypkiewicz ^{1,2} ,
Michal Wierzbicki ^{1,2,3}, Agnieszka Zurawska ^{1,2}, Arkadiusz Baran ^{1,2,3} , Maciej Bakala ^{1,2,3}
and Jakub Kupecki ^{1,2,4}

¹ Institute of Power Engineering, Mory 8, 01-330 Warsaw, Poland; marcin.blesznowski@ien.com.pl (M.B.); marek.skrzypkiewicz@ien.com.pl (M.S.); michal.wierzbicki@ien.com.pl (M.W.); agnieszka.zurawska@ien.com.pl (A.Z.); arkadiusz.baran@ien.com.pl (A.B.); maciej.bakala@ien.com.pl (M.B.); jakub.kupecki@ien.com.pl (J.K.)

² Center for Hydrogen Technologies (CTH2), Institute of Power Engineering, Augustowka 36, 02-981 Warsaw, Poland

³ Institute of Heat Engineering, Warsaw University of Technology, Nowowiejska 21/25, 00-665 Warsaw, Poland

⁴ National Fuel Cell Research Center (NFCRC), University of California, Irvine Engineering Laboratory Facility, Irvine, CA 92697-3550, USA

* Correspondence: konrad.motylinski@ien.com.pl; Tel.: +48-797-905-192

Received: 28 September 2020; Accepted: 27 October 2020; Published: 29 October 2020



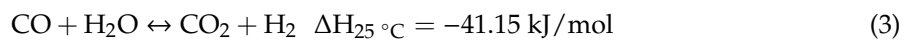
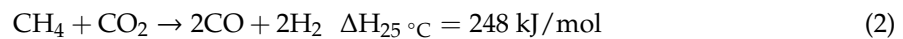
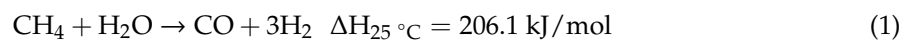
Abstract: Solid oxide fuel cells (SOFCs) can be fueled with various gases, including carbon-containing compounds. High operating temperatures, exceeding 600 °C, and the presence of a porous, nickel-based SOFC anode, might lead to the formation of solid carbon particles from fuels such as carbon monoxide and other gases with hydrocarbon-based compounds. Carbon deposition on fuel electrode surfaces can cause irreversible damage to the cell, eventually destroying the electrode. Soot formation mechanisms are strictly related to electrochemical, kinetic, and thermodynamic conditions. In the current study, the effects of carbon deposition on the lifetime and performance of SOFCs were analyzed in-operando, both in single-cell and stack conditions. It was observed that anodic gas velocity has an impact on soot formation and deposition, thus it was also studied in depth. Single-anode-supported solid oxide fuel cells were fueled with gases delivered in such a way that the initial velocities in the anodic compartment ranged from 0.1 to 0.7 m/s. Both cell operation and post-mortem observations proved that the carbon deposition process accelerates at higher anodic gas velocity. Furthermore, single-cell results were verified in an SOFC stack operated in carbon-deposition regime by dry-coupling with a downdraft 150 kWth biomass gasifier.

Keywords: Boudouard reaction; carbon deposition; SOFC

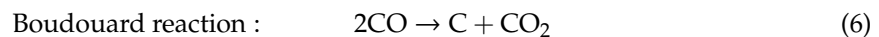
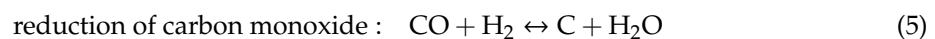
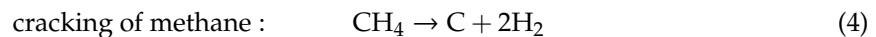
1. Introduction

One of the key advantages of solid oxide fuel cells (SOFCs) is their fuel flexibility. The ability to convert hydrogen, carbonaceous, and hydrocarbon fuels privileges the application of these devices in energy transition technologies, where high efficiency and environmentally-friendly parameters must be secured. The elevated operating temperature in the range from 600 °C to 850 °C enhances the electrochemistry, catalyses chemical reactions, and guarantees usability of heat at the outlet of the SOFC unit [1]. This heat is used to preheat incoming streams of gases entering the fuel cells and can be used in the preparation of hot water or steam in cogenerative systems [2] or, optionally, can be used to drive an absorption chiller for the production of cold [3]. With these approaches SOFCs can be considered as

prime movers in electricity generators, combined heat and power units (CHP), and combined heat, power and cooling systems (CCHP). Systems with SOFCs can be part of systems which enable carbon recovery and recycling for zero net carbon dioxide emissions by integration with algal systems for CO₂ utilization [4]. They can be employed in carbon capture and sequestration (CCS)-ready systems which integrate post-combustion processes of anodic lean gases with oxygen membranes to achieve high concentrations of carbon dioxide in exhaust gases [5]. These benefits make this technology attractive for stationary applications [6]. SOFC-based power units are characterized by electrical efficiency of 45% to 65%, whereas 37–45% is reported for conventional steam-cycles [7–9] and up to 60% for state-of-the-art natural gas combined cycles (NGCC). The electrical efficiency of systems with SOFCs can be elevated by fuel recirculation or by serial connection of fuel cell stacks [10]. Moreover, processes like waste incineration [11], anaerobic digestion [12], biomass gasification, and pyrolysis produce gases which can fuel SOFC plants [13–15]. For such fuels, minimal pre-processing like desulfurization [16,17] and pre-reforming [18] are required. Currently, such gases are mainly combusted in burners designed to accept the presence of hydrogen and impurities. SOFCs mitigate or avoid some of these problems, due to fuel conversion inside the cell. The anode's catalytic properties and the high operating temperature promote internal steam reforming of hydrocarbons like steam methane reforming (SMR) (Equation (1)) [19], dry reforming of carbon dioxide and methane (Equation (2)), [20] and the water gas shift reaction—WGS (Equation (3)) [21].



Apart from the many benefits of Ni-YSZ cermet, it also favors the formation of solid particles of carbon over its surface [22]. A nickel-based electrode is a very good catalyst for carbon formation reactions, such as the following:



The increase of CO concentration in fuel enhances carbon deposition via the Boudouard reaction in the anode volume, as well as other stack elements and pipelines [23]. A similar effect is obtained when the SOFC is fueled with pure methane or methane-rich gases, due to the methane cracking reaction. Usually, tests with demanding fuels are performed by operating at high current densities in order to promote WGS reaction [24], higher fuel utilization [25], and at appropriate steam-to-carbon ratios (S/C) in order to keep carbon activity at near unity. Setting an appropriate S/C value helps to create operating conditions in which carbon deposition is thermodynamically unfavored. In typical SOFC power generation systems, the S/C ratio value is set to 2.2, as shown in Figure 1 [26–28]. One way to determine a safe value for this process is to use ternary diagrams with isotherms of carbon formation or Gibbs diagrams (Figure 1). The thermodynamic boundary between non-deposition and deposition zones can be defined by determining the equilibrium composition for different gas mixtures, containing carbon, hydrogen, and oxygen atoms. Curves for different temperatures are presented in the diagram as isotherms of carbon formation [29].

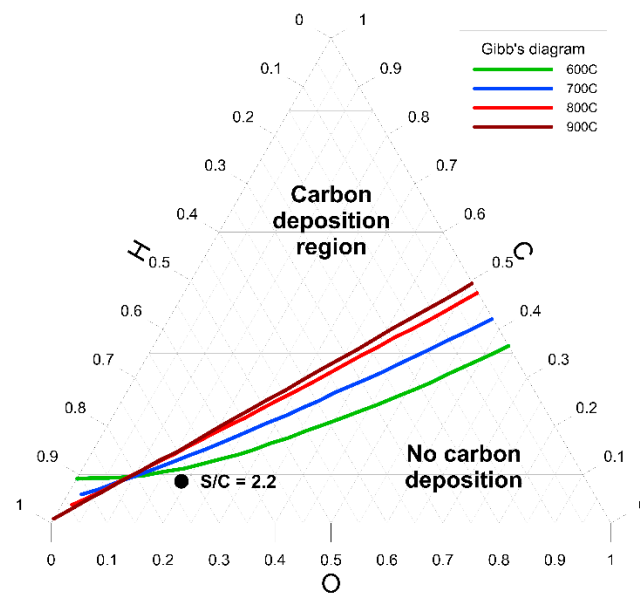


Figure 1. Gibbs triangle for steam reforming of methane with steam-to-carbon ratios (S/C) ratio of 2.2 (based on [30]).

Carbon deposition might occur in various conditions. Firstly, the formation of a solid carbon layer on the porous surface might affect the uniformity of flow distribution along the active area of the fuel cell [31]. Moreover, the thin layer of deposit leads to reduction of the active area or triple phase boundary (TPB) length involved in high temperature electrochemical processes [32]. In addition to affecting the outer surface, it can lead to an increase of exposure time to a significant deterioration of the physical and chemical properties of the material and functional layer of the anode [33].

Numerous groups applied the electrochemical impedance spectroscopy (EIS) technique for determining the cell parameters and degradation in methane-fueled anode-supported SOFCs. Chen et al. [34] demonstrated that operating conditions and composition of fuel influence the morphology of deposited carbon structures and the fuel cell degradation process. Their EIS measurements revealed that for the fuel cell with a Ni-YSZ anode fueled with syngas, the cell electrochemical performance degraded very rapidly after carbon was deposited. Koh J. et al. [35] presented that carbon deposition with humidified methane on a Ni-YSZ porous surface is reversible when it is oxidized at a current load in thermo-dynamically carbon-free conditions. They measured a short-term (3 h) EIS evolution on a Ni-YSZ anode-supported cell fueled by a mixture of methane and nitrogen. The EIS measurement was realized under carbon-deposition-promoting conditions—at open circuit voltage (OCV) as well as at load, beyond the carbon deposition regime. The spectrum at OCV evolved strongly, especially in the beginning of the experiment. Operation at current revealed a stable spectra for 100 min. Lanzini et al. [32] investigated a Ni-YSZ-supported cell (diameter 80 mm) with a mixture of methane and CO₂ for 250 h. Up to 200 h, the spectra change was linear and rather limited. After 200 h, carbon deposition caused a dramatic increase of the cell's area-specific resistance (ASR), leading the experiment to an end. Lyu et al. [36] investigated direct internal reforming (DIR) of methane and published EIS spectra of the anode-supported SOFCs (AS-SOFCs) tested at various S/C ratios. S/C above 0.5 revealed very good DIR-SOFC performance. Decreasing S/C to 0.5 and further (down to 0.03) resulted in a high ASR increase. From the reported data, lowering S/C slightly decreased cell ohmic resistance. Silva-Mosqueda et al. [37] investigated an AS-SOFC for 500 h, measuring impedance spectra. During the operation, an increase in the cell impedance was observed mainly in the intermediate frequencies. Papurello et al. [38] investigated steam-reforming of simulated biogas (60% methane, 40% carbon dioxide) inside an SOFC anode. Numerous impedance spectra were presented including a mild H₂S poisoning of the cell at 750 °C for 10 days (S/C = 1.0, 0.46 ppm H₂S). The ohmic cell resistance

decreased in time while the ASR increased significantly, which was addressed to sulfur poisoning and to a smaller extent, to carbon deposition. Several publications mention different types of dopants that inhibit the carbon deposition process without influencing fuel cell performance [39–43].

The aim of this work is to compare the soot deposition mechanisms on the fuel electrode in a single-fuel-cell and stack environment in order to determine the correlation between operating parameters and cell degradation. Moreover, the results demonstrate the acceptable deviations from theoretically-safe fuel cell operating conditions.

2. Experimental Setup

To experimentally study carbon formation on the surface of nickel-based electrodes exposed to carbon-rich fuels, two approaches were proposed within the testing campaign. The first approach concerned single-cell experiments whereas the second one—the stack environment. In both cases, anode-supported SOFCs (AS-SOFCs) were used. However, the active area and thickness differed. In the case of a 1-mm-thick single cell, the active area was 16 cm². A 5-cell stack was comprised of 0.55 mm thick cells with 92 cm² of active area per cell.

The experimental setups were operated in test stands consisting of an electric oven, gas analyzers (Siemens, Munich, Germany), electrochemical workstation (Zahner IM6ex+PP240, ZAHNER-elektrik, Kronach, Germany), electronic load (Chroma 63201, Chroma, Xiamen, China), and data acquisition system (temperatures, pressures, and voltages). The construction of the test stands differed in detail but provided similar functionality. In contrast to single-cell testing, the AS-SOFC stack was fueled in operando by syngas from a gasifier.

2.1. Single-Cell Testing

In the present work, custom-made planar AS-SOFCs (50 × 50 × 1 mm, 16 cm² active area) produced at the Institute of Power Engineering, Ceramic Department CEREL were used in the experimental analysis for single-cell testing [44,45]. A cross-section of the cell is shown in Figure 2 together with definitions of particular layers.

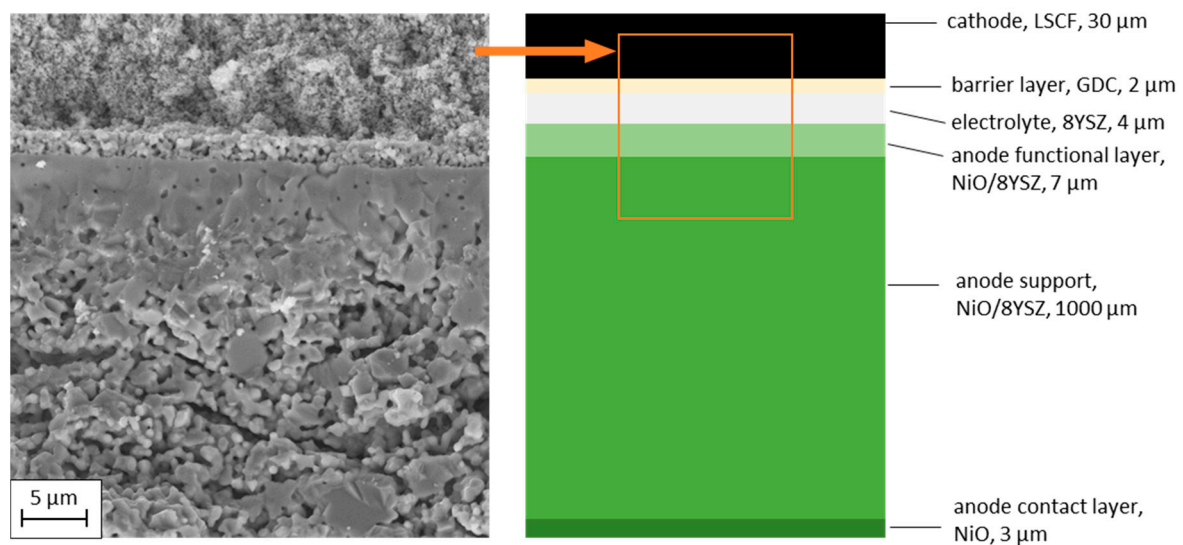


Figure 2. Microstructure of the analyzed anode-supported solid oxide fuel cell (AS-SOFC) and a diagram of the cell's composition.

Alumina housing was used in the experiments. The cells were placed between two gold current collectors. A schematic diagram of the complete test stand is shown in Figure 3.

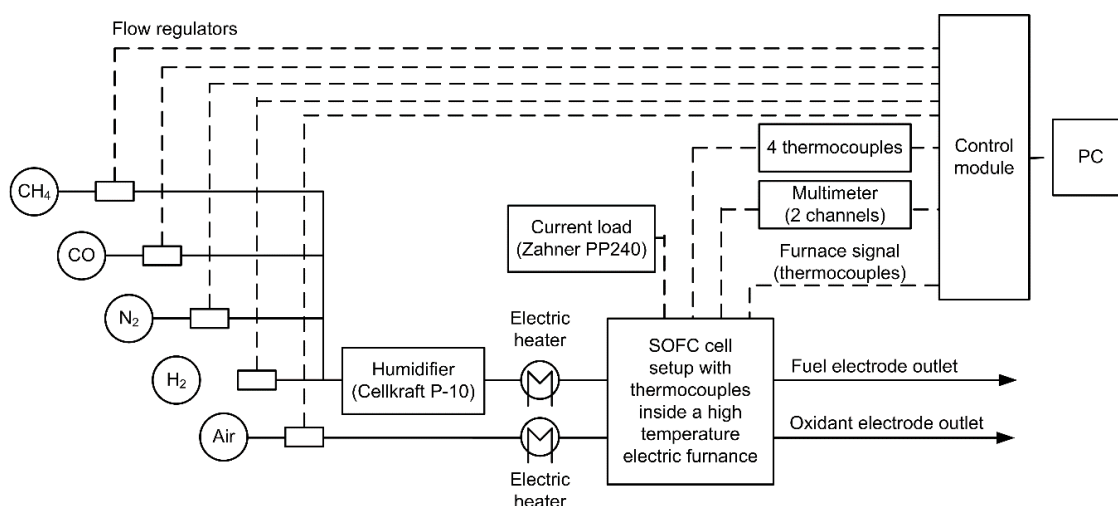


Figure 3. Schematic diagram of single-cell testing stand.

The furnace temperature during experimental characterization of single cells was constant at 750 ± 1 °C. Initially, internal reforming in the cell was analyzed in terms of carbon deposition occurring due to the insufficient amount of steam in relation to the fuel supplied. The flow of pure methane (50 NmL/min, methane 5.0, Messer, Poland) was initially humidified at 88 °C using a Cellkraft P-10 humidifier, before entering the fuel cell housing. During the experiment, the steam-to-carbon ratio was gradually decreased from 2.0 to 0.15 by decreasing the humidification temperature, with a step change of approximately 0.1. This approach is equivalent to a situation in which the steam delivering module underperforms, the fuel flow control fails, or a steam leakage occurs. As a result, less H₂O is mixed with the fuel. The current load was set at a constant level of 2A for the whole test, which lasted 1000 h. The degradation of the cell was monitored on-line and additionally using electrochemical impedance spectroscopy (EIS), while postmortem analysis was done using a scanning electron microscope, JEOL JSM-6010PLUS/LA (SEM).

Additionally a different hypothesis, stating that fuel gas velocity might also affect the carbon deposition process, was analyzed in parallel to the first tests of the experimental campaign. In these cases, constant gas composition of the anodic inlet gas was composed of 12.5% H₂, 37.5% CO, and 50% N₂, without any addition of steam. Knowing the geometry of the gas channels in the housing and the composition and flow of the fuel, its initial velocity could be calculated. In the performed experiments, anodic gas flow in the range from 120 NmL/min to 640 NmL/min, corresponding to 0.1 m/s and 0.7 m/s, respectively, was analyzed experimentally. Six independent tests were performed—three runs at constant current 3A and an additional three experiments in open circuit voltage conditions. Excluding cell reduction, heating and cooling, the observation of cell performance was conducted for 7 h of measurements per case. This length allowed clear observation of carbon deposition in both in operando measurements as well as postmortem samples. For each experiment, EIS measurements were performed in order to determine SOFC degradation over time under constant electric load.

Additionally, after completing the experimental campaign, the last test with a single cell was realized. It aimed to monitor cell performance degradation in the same conditions, but for 200 h instead of 7 h.

2.2. Stack Testing

The analysis of carbon deposition in the 5-cell stack was done using custom-made anode-supported cells composed of the following layers: Ni-YSZ|YSZ|GDC|LSC. The stack was composed of interconnects made of ferritic stainless steel with composite glass seals which were manufactured and assembled in SOFC/SOE stack production facilities of CTH₂. The fueling gas was produced in the gasifier, in a similar manner to that presented by Subotic V., et al. [46].

The gasification system included a buffer tank for the feedstock, a screw feeder, the KAJOT gasification reactor [47], a cyclone-based separator of fine particles installed downstream of the gasifier, a heat exchanger of flue gas, and fans for continuous gas supply. Volatile matter, released from the feedstock in the pyrolysis step, was burned in the first section. Combustion reactions were exothermic and the heat generated during this step was delivered to the drying/pyrolysis stage and to the gasification zone in order to sustain the endothermic gasification reactions.

In the test the feedstock was common hardwood wood chips composed of an alder and beech mixture in a 50/50 ratio. The dimensions of the wood chips were ca. $10 \times 10 \times 3$ mm. In the experiment air was used as a gasifying agent. The volatile matter released from the heated-up feedstock burns in a separate chamber in the reactor and the flue gases produced heat up the gasifying agent through a heat exchanger. In the second zone the main process of gasification takes place. The gas generated is composed mainly of flammable gases CO, H₂, CO₂, CH₄, N₂ used as an inert gas, and H₂O. However, the gasification product gas contains trace amounts of other contaminants such as particles, tars, and sulfur compounds in the form of H₂S and COS. The type and amount of contaminants relate to the type of biomass feedstock, temperature of the process, gasifying agent, residence time, equivalence ratio, and type of gasifier [48]. A cyclone was installed downstream of the reactor to separate solid particles from the gas. During the experiment, average fuel flow was 9.49 kg/h and average cold gas efficiency (CGE) was 68.5%. A small part of the gas was transported through a heated (200 °C) line to the SOFC stack. The main part of the gas stream was burned in a separate combustion chamber. A schematic diagram of connection is presented in Figure 4.

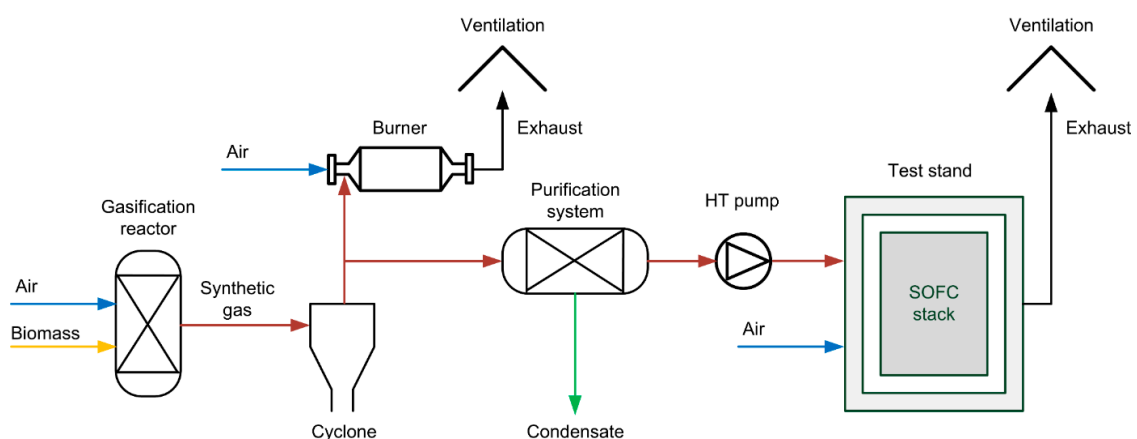


Figure 4. Schematic diagram of system connections.

The stack was operated in a test stand consisting of an electric oven, gas analyzers, electrochemical workstation (Zahner IM6ex+PP240—used for selected cell EIS measurements), electronic load Chroma 6310A, and data acquisition system (temperatures, pressures, and voltages). The test setup scheme is presented in Figure 5.

During the first heat up, the stack was compressed at elevated temperature in order to obtain gas-tightness. Then the procedure to reduce nickel oxide was initiated. This stage of experiment was performed with reference fuel, which is a mixture of hydrogen and nitrogen. After conducting the initial measurements of stack performance and verifying gas-tightness, the stack fuel source was switched from the hydrogen/nitrogen mixture to the gasification product gas from the KAJOT gasifier. The air flow through the stack was kept constant at 10 Nl/min throughout the whole test run.

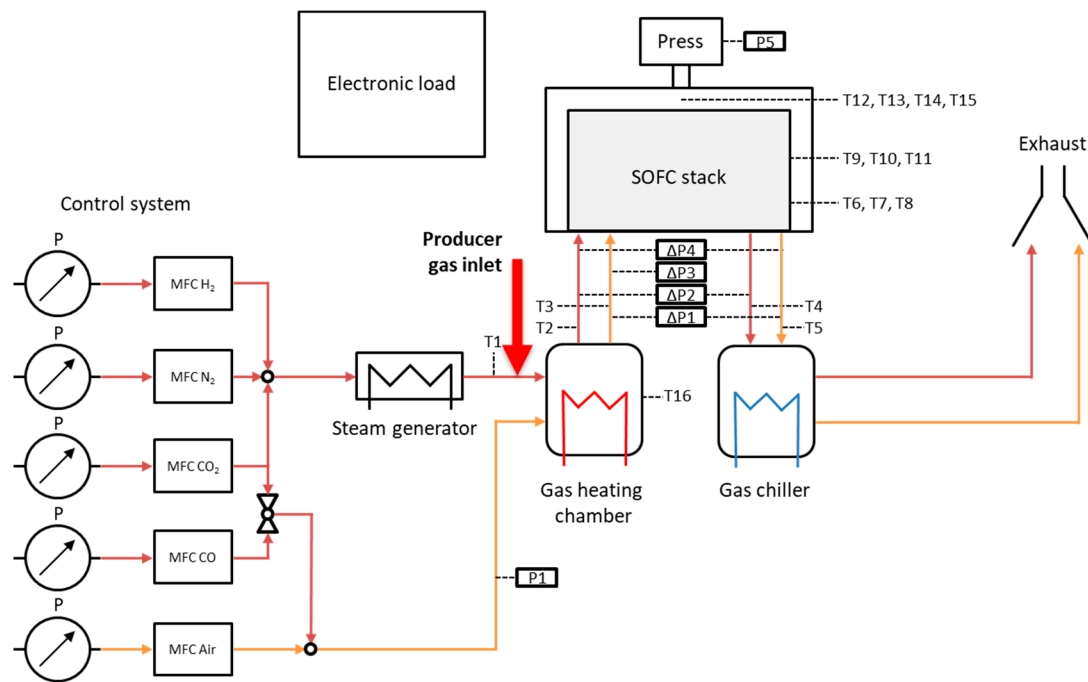


Figure 5. Short stack testing setup scheme.

The experiment was conducted under constant current load, which was initially set at 25 A, but after a few hours of operation the load was decreased to 20 A and remained constant to the end of the experiment. During the test, stack temperature was kept constant at 680 °C with variations of ± 0.5 °C.

The flow of fuel has been maintained with a high temperature pump operated at 180 °C equipped with a manual control valve. Regulation of the flow was done periodically, every 120 min with a manual flowmeter at the stack outlet to keep the fuel utilization (FU) coefficient at a constant 8%. The flow was maintained at $3 \div 3.5$ Nl/min depending on the content of hydrogen, carbon monoxide, and methane in the producer gas. It is important to note that while no significant fluctuations of the flow were observed throughout the one-week test campaign, the composition of gas fluctuated slightly and therefore the flow had to be adjusted to keep the FU unchanged.

3. Results and Discussion

3.1. Single SOFC

Numerous EIS measurements were performed during the 1000 h test with decreasing amounts of steam delivered. A reference sample of measured spectrum for a steam-to-carbon ratio of 0.88 is shown in Figure 6. The EIS comparison for different S/C ratio values is shown in Figure 7.

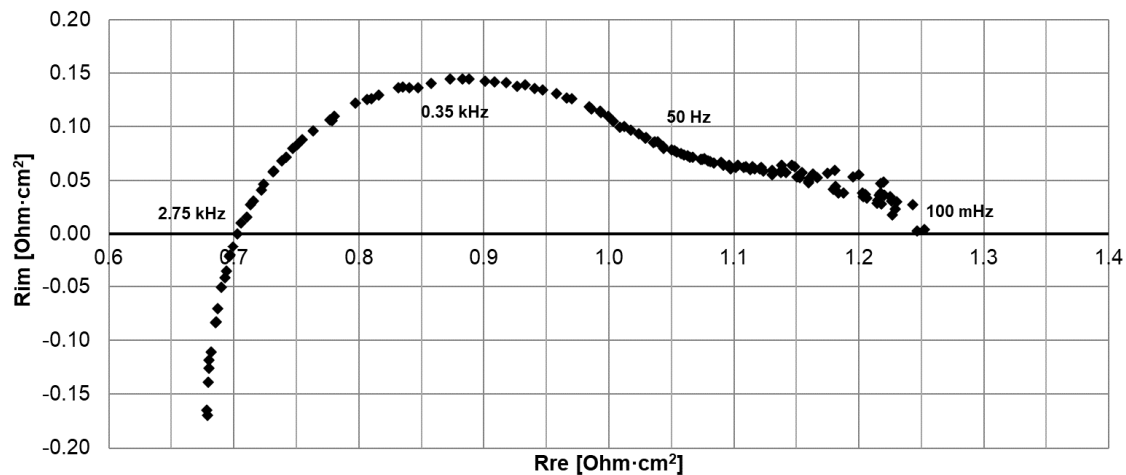


Figure 6. electrochemical impedance spectroscopy (EIS) of tested single cell at S/C = 0.88 at 750 °C and 0.9 V, amplitude 10 mV.

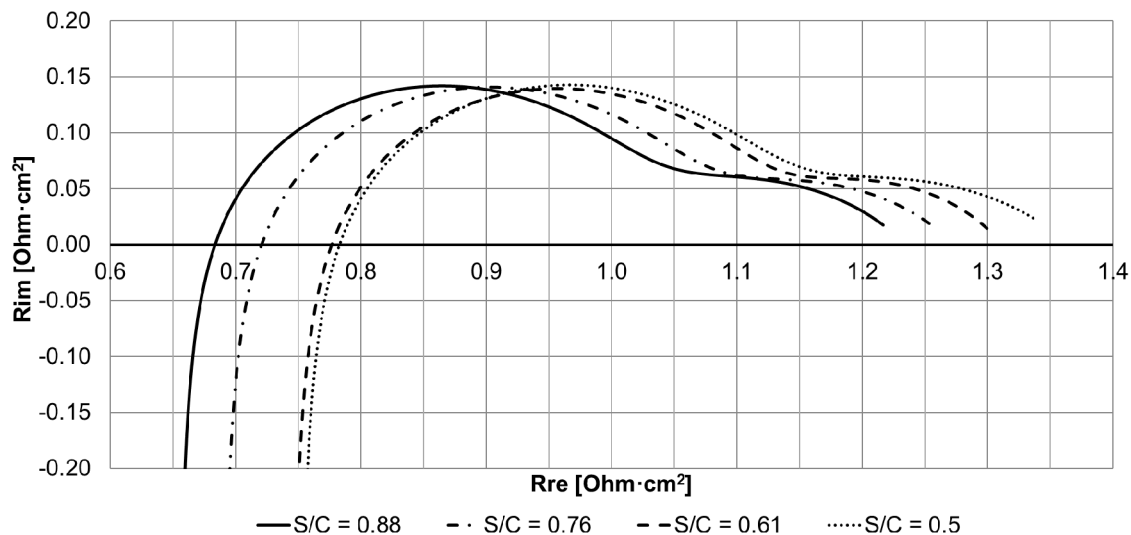


Figure 7. EIS comparison for different S/C generated by in-house codes for linear visualization of spectroscopy measurements at 750 °C and 0.9 V, amplitude 10 mV.

The collected data shows that the decrease in S/C was followed by an increase in the resistance of the fuel cell, but without the qualitative changes in the impedance pattern. These changes can be described as two RQ arcs with RL chain in high frequencies (similar to those presented in [49]).

For the realized EIS, both ohmic cell resistance and cell area-specific resistance (ASR) were determined. For the performed spectroscopy measurements on the SOFC, resistance values below 10 Hz were distorted, as shown in Figure 6. As a result, it was difficult to accurately determine the actual area specific resistance, but it can be assumed that cell ASR was similar in each case. Observed distortions on low frequencies were caused by several processes occurring simultaneously in the anodic compartments of the SOFC including partial direct steam reforming (highly endothermic), electrochemical oxidation (highly exothermic), and formation of carbon particles. Similar effects were observed by Subotic et al. [50]. With each drop of S/C value, ohmic cell resistance of the SOFC increased, thus showing the undesirable changes in cell structure. The correlation between DC cell ohmic resistance (referred to as R1), ASR, and steam-to-carbon ratio is presented in Figure 8.

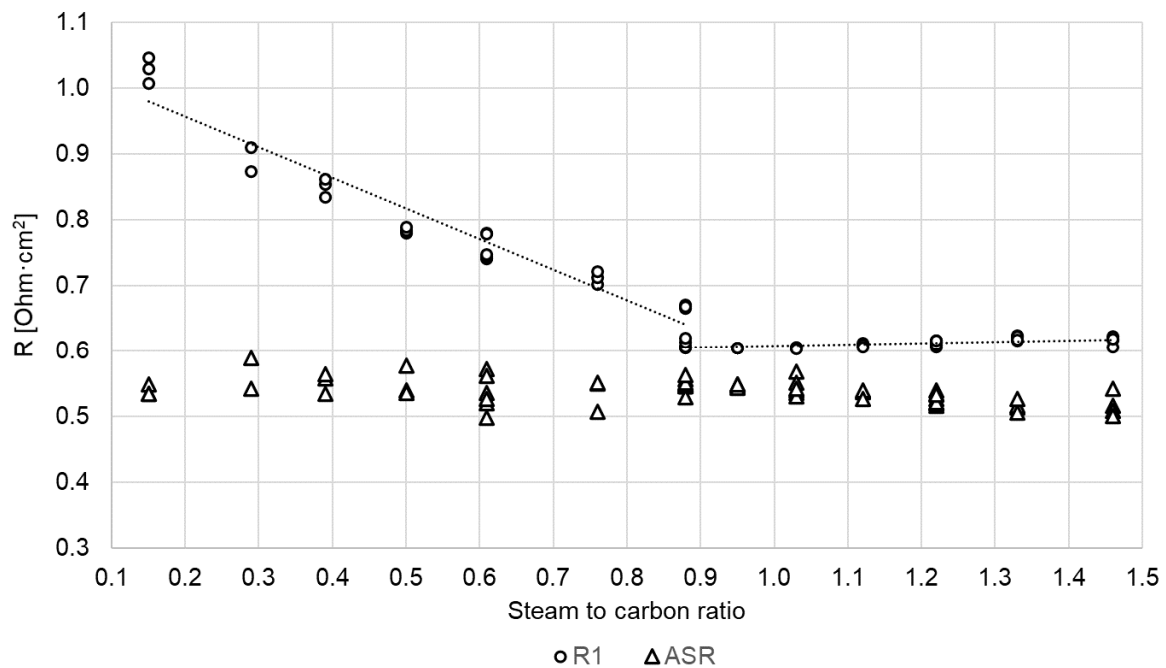


Figure 8. Ohmic cell resistance (R1) and area-specific resistance (ASR) with respect to S/C.

During the 1000 h-long experiment, cell voltage was also measured. It is presented in Figure 9.

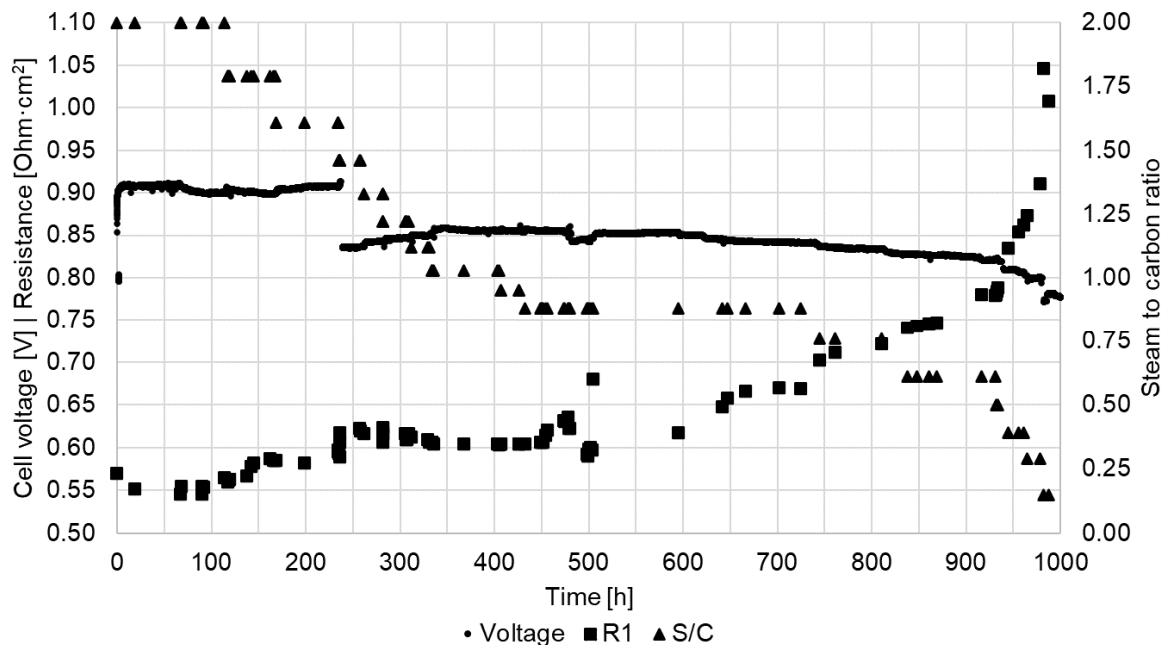


Figure 9. Measured fuel cell voltage and ohmic resistance evolution with decreasing S/C during 1000 h experiment. At 240 h the load was doubled from 1 A to 2 A.

Additionally, both cell resistance and steam-to-carbon ratio were also presented in the graph. The major voltage drop of around 240 h was caused by the change of electric load from 1 A to 2 A, due to the fact that for smaller current, cell was operating in the activation area. Initially, with lower amount of steam, cell performance was better, caused by the less-diluted fuel delivered to the cell. Eventually, voltage drop started when S/C was equal to 0.88, resulting in damaging the cell, which was also observed by a significant increase of cell resistance. Further lowering the steam-to-carbon ratio caused accelerated cell performance degradation.

With a lower amount of steam delivered, a bigger role was taken by the soot-formation reactions—a lower S/C ratio results in the deflection of the equilibrium of the Boudouard reaction (Equation (6)) in favor of carbon deposition and increased activity of the carbon monoxide (according to Equation (3)). Also steam oxidation of the carbon deposits (Equation (5)), including nucleuses of the solid phase, becomes more unlikely. Boundary values for S/C can be found on Figure 1. The postmortem analysis showed that at low S/C conditions serious cracks occurred near the fuel inlet during the test. Likely it is a synergetic effect of the thermal stresses, induced by endothermic steam conversion of the methane (Equation (1)) and growth of the carbon deposits on the anode support. It is necessary to mention here that more prominent evidence of the cell destruction were observed on the cathode side, due to leakage of the fuel through cracks in the cathode compartment, which led to delamination of the Lanthanum Strontium Cobalt Ferrite (LSCF) layer. However, SEM analysis demonstrated existence of the dense net of the crack in the anode support. Only the biggest of these cracks is likely to reach the cathodic side of the cell. Figure 10 presents the state of the SOFC near the fuel inlet after the 1000-h experiment with decreasing S/C ratio.

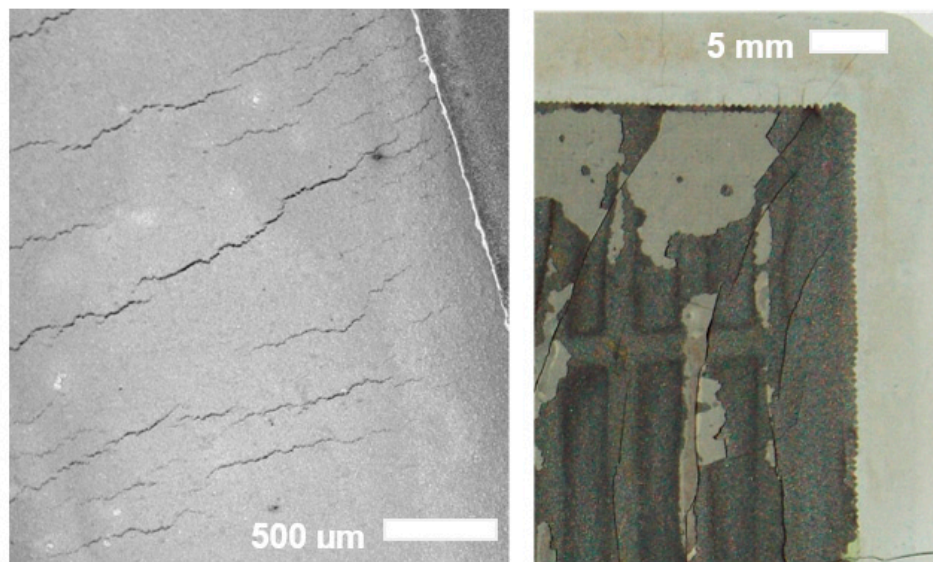


Figure 10. Cracks near the fuel inlet. (Left), SEM of the anode support; (right), image of cathode, delaminated due to fuel leakage.

For the experiments with simulated reformat at different velocities, postmortem observations are shown in Table 1.

Table 1. Carbon deposition for various anode gas velocities at 750 °C and S/C = 0.

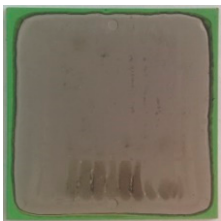
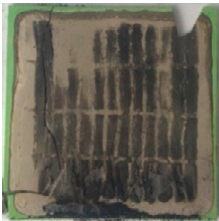

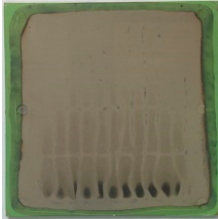
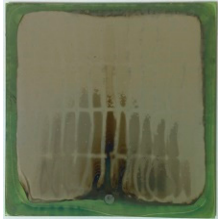

Velocity	0.1 m/s	0.3 m/s	0.5 m/s	0.7 m/s
OCV				-

Table 1. Cont.

Velocity	0.1 m/s	0.3 m/s	0.5 m/s	0.7 m/s
3A	-			

The results obtained prove that gas velocity correlates with the carbon deposition process. When the SOFC works in OCV conditions, formation of carbon solid particles is more intense than when it operates under current load. As a result, a low amount of steam and a high concentration of CO favors the decomposition of CO in the Boudouard process (Equation (6)).

The results for the extended test (200 h) are shown in Figure 11. The initial time corresponds to the start of carbon deposition. Initially, the experiments were performed for 0.7 m/s initial, anodic gas velocity.

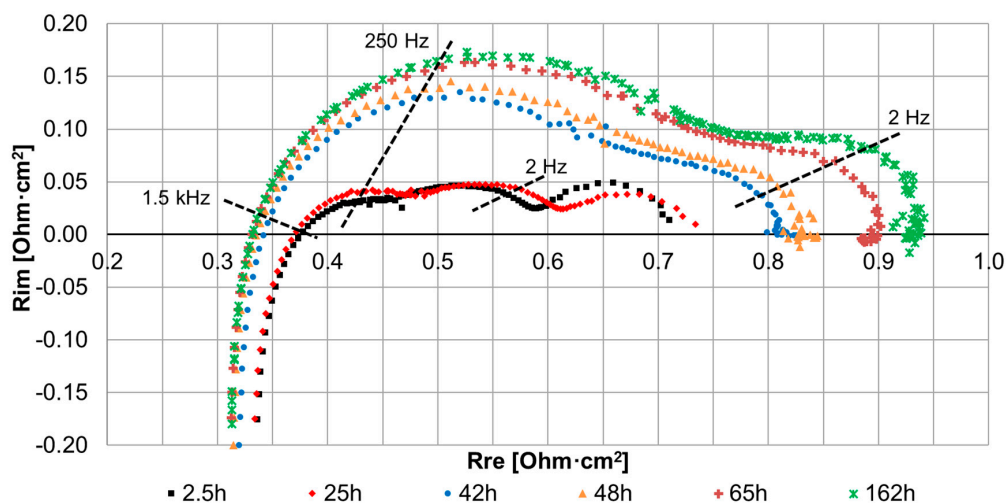


Figure 11. Impact of soot formation on fuel cell degradation—selected results of the EIS measurements. Data recorder under initial gas velocity of 0.7 m/s at 750 °C, amplitude 10 mV.

As presented in Figure 11, it was observed that fuel cell electrochemical performance was highly dependent on the carbon deposition process. During the first 24 h of operation after the switch of fuel from H_2-N_2 to the $CO-H_2-N_2$ mixture, degradation was minor and was observable only by some evolution of EIS spectra and minor decrease in voltage equals ca. 4.3 mV. In the next phase, the transition process occurred and led to a significant drop in voltage. The duration of transition was approximately 48 h, during which the resistances that may be attributed to the electrochemical processes increased (including cathodic), resulting in the increase of ASR of the cell from ca. $0.34 \Omega \times cm^2$ at the beginning of the experiment up to ca. $0.6 \Omega \times cm^2$ at its termination. Simultaneously the ohmic resistance fell slightly from ca. $0.38 \Omega \times cm^2$ (initially) down to ca. $0.33 \Omega \times cm^2$. The latter phenomenon may be explained as enhancement of the contact between anode and the current collector due to deposition of carbon particles which exhibit good conductivity. Similar phenomena were to some extent observed by Lyu et al. [36]. The rise in cathodic polarization may be explained through the exclusion of the soot-covered area of the cell from transport of electric current. Slow degradation was observable even after 162 h of operation.

The complex nature of the observed phenomena (anode degradation, blocking of the cell surface from charge transportation, etc.) meant that we were unable to create a tolerable model for equivalent circuits to describe the evolution of the impedance spectra. The degradation of the fuel cell caused by carbon deposition can be divided into three characteristic zones, as presented in Figure 12.

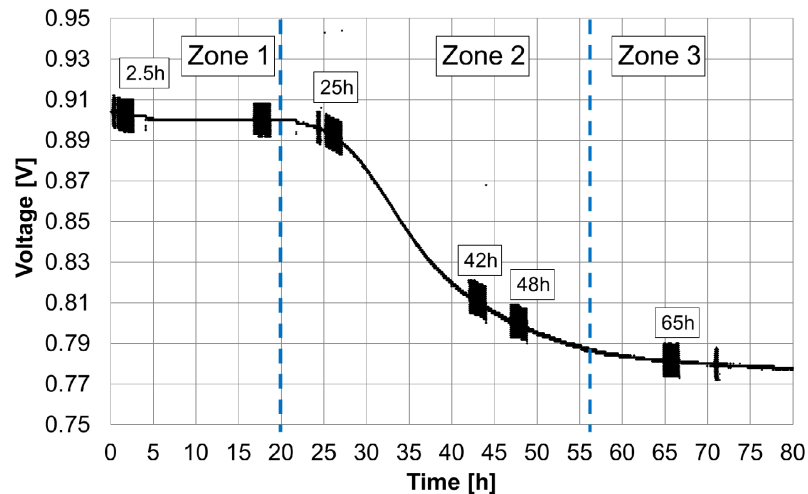


Figure 12. Impact of soot formation on fuel cell degradation—evolution of voltage. Data recorded at initial gas velocity of 0.7 m/s at 750 °C and constant current 3 A, visible EIS measurements with amplitude 10 mV.

In Zone 1 approximately 23–24 h degradation of ca. 180 mV/1000 h was observed. The most aggressive degradation appeared in Zone 2, where the voltage dropped by ca. 120 mV in less than 48 h. The degradation rate in Zone 3 was similar to Zone 1, with a low degradation rate of ca. 170 mV/1000 h. It can be concluded that the carbon formation and deposition process started at the beginning of Zone 2. After solid carbon particles blocked the pores of the anode, there was no further observable impact of soot deposition on fuel cell performance and a return to slow degradation ensued in Zone 3.

The same analysis was performed for the other initial fuel velocity values: 0.3 m/s and 0.5 m/s. Both values of OCV and cell voltage at 3 A load were different for each anode gas velocity case, thus a different approach was proposed for comparison purposes. In Figure 13, voltage drops were shown with reference to the initial value of each experiment. The dots in the chart represent the actual voltage drop measurements, while the thin lines are approximations for visualization purposes only.

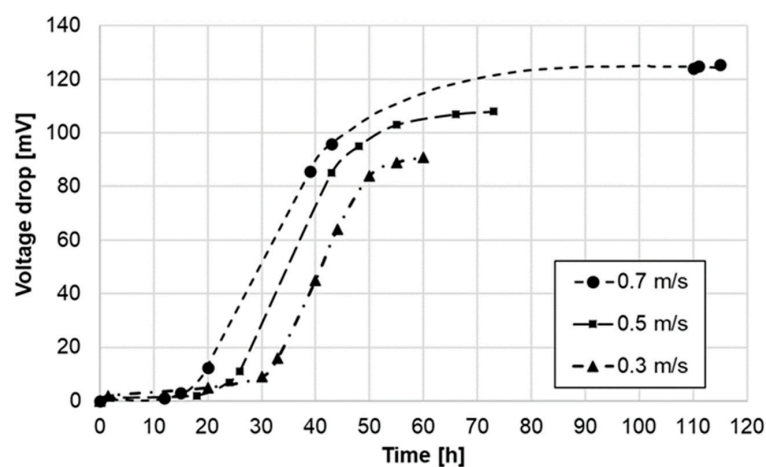


Figure 13. Fuel cell voltage drop at constant current load 3 A recorded for three different values of initial gas velocity in the anodic compartments at 750 °C.

Based on the analysis of the results it can be concluded that a similar degradation rate was observed during each of the experiments. Taking into account the measurements, the time after the fuel cell that rapid degradation begins (transition from Zone 1 to 2) can be correlated with the anode gas velocity according to:

$$t_{cd} = -37.5v^2 + 90v - 20.625 \quad (7)$$

where t_{cd} is time elapsed after which the rapid fuel cell degradation caused by carbon deposition starts and v is the anodic gas velocity.

Because the high anode thickness (1 mm) clearly damps the dynamics of performance degradation, the formula might be amended by factoring in the thickness of the anode.

3.2. SOFC Stack

Before fueling the SOFC stack with producer gas from a prototype, two-section, downdraft gasifier, KAJOT, the initial stack performance was measured. The reference curve was obtained for the hydrogen/nitrogen mixture (Figure 14). Power density at 0.9 V was $\sim 0.275 \text{ W/cm}^2$ and cell ASR calculated from the I–V curve between 0.9 and 0.85 V for a representative fuel cell in the stack (no 3) was $0.36 \Omega \times \text{cm}^2$.

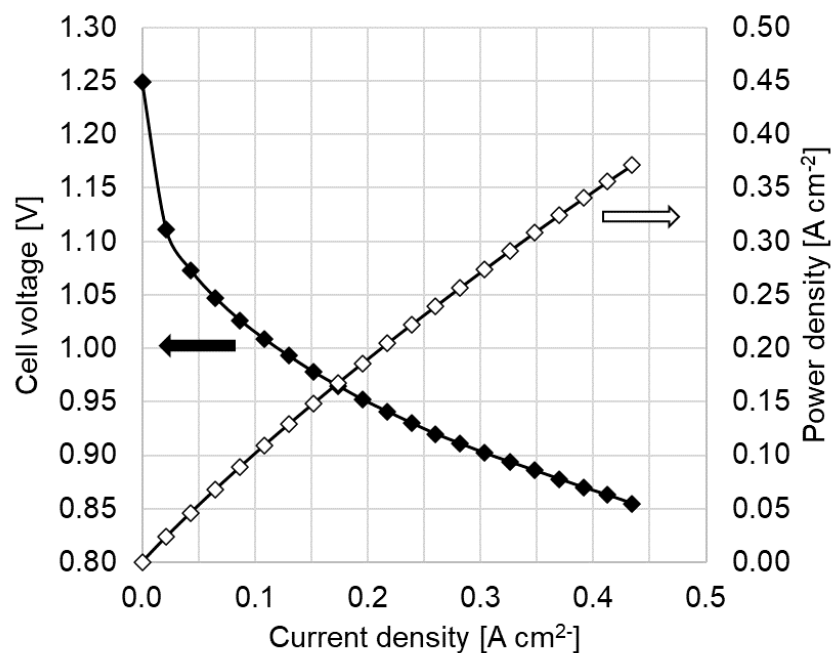


Figure 14. U-I reference curve for cell no. 3 in 5-SOFC stack. Oxidant: air. Fuel: 50% H₂ and 50% N₂ mixture at 680 °C.

Afterwards the stack fuel source was switched from the hydrogen/nitrogen mixture to the gasification product gas. Gas composition fluctuated throughout the test. The representative composition of the producer gas together with observed fluctuations is presented in Table 2.

Table 2. Composition of syngas excluding trace compounds.

Component	Molar Concentration
H ₂	18 ÷ 21%
CO	21 ÷ 25%
CO ₂	8.5 ÷ 11%
CH ₄	1.5 ÷ 2%
O ₂	0%
N ₂	38 ÷ 41%
H ₂ O	8 ÷ 10%

To gain deeper understanding of the fuel composition from the carbon deposition point of view, Gibbs triangle with isotherms of carbon formation was prepared. Average syngas composition was used in order to determine the operating point, which is presented as a red dot in Figure 15. Mathematical calculations proved that the operating temperature (680 °C) together with the wet gas composition (8% water content) was very close to the isotherm which separates the safe operating zone from the operating conditions at which carbon deposition thermodynamically occurs. The test with producer gas was conducted under current load with current density of ca. 0.2 A/cm², equivalent to the one applied in the tests for the 50 mm × 50 mm cells. This produced comparable conditions in terms of the carbon deposition process in both environments—small single cell and the stack fueled by real fuel.

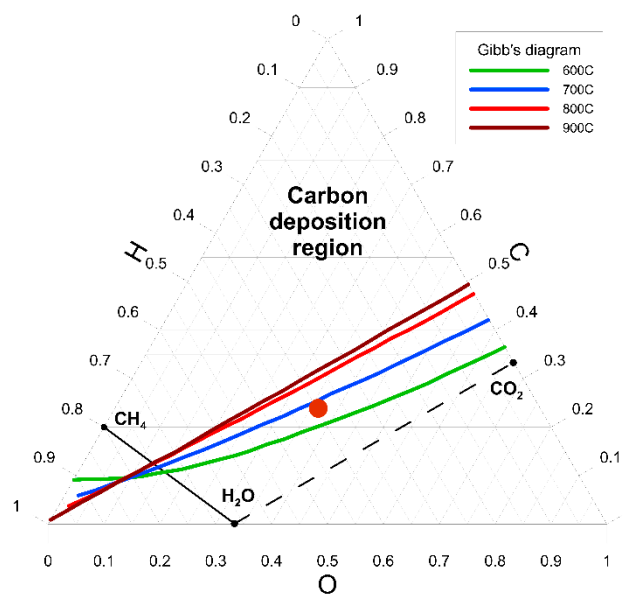


Figure 15. Gibbs triangle for steam reforming of methane with red dot highlighting the operating point in case of produced syngas from the KAJOT gasifier.

During the first 18 h of operation on gasification product gas, the degradation rate was quite low, but later it started to be destructive (ca. 1250 mV/1000 h). Figure 16 demonstrates the loss of performance of a representative cell from the 5-cell stack as a result of operation on the gasification-derived fuel for 120 h. After this period, the stack was cooled and the postmortem analysis phase started.

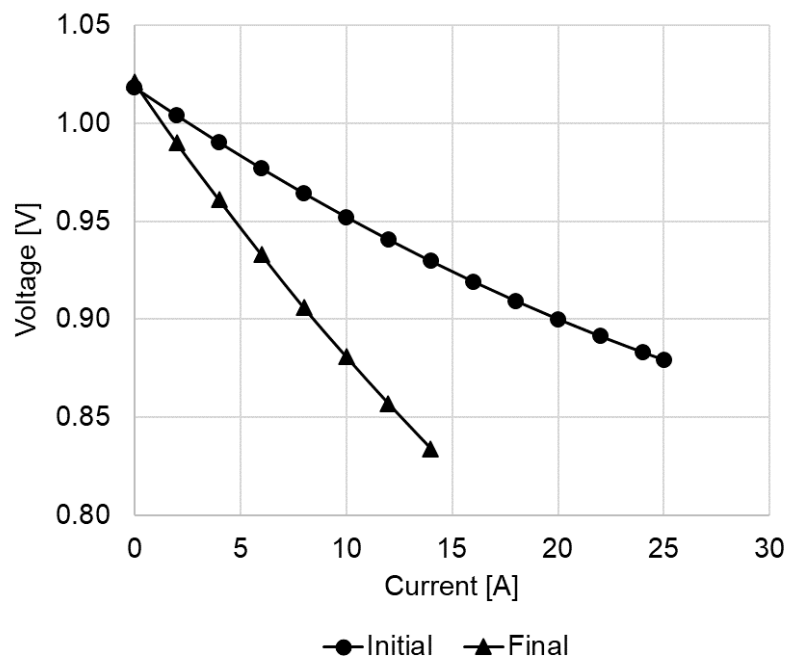


Figure 16. U-I curve for cell no. 3 in 5-cell SOFC stack at start and end of syngas supply. Oxidant: air. Operating temperature 680 °C.

The investigation proved that an intense carbon deposition process occurred during the test. Figure 17a,b, presenting a view of the anode support edge adjacent to the fuel inlet, demonstrated heavy carbon deposition on the anode of a representative cell. It looked similar in other cells.

Analysis of the experiment data and postmortem results reveal three independent facts impacting the carbon deposition processes:

- thermodynamics at least close to the boundary of the heterogenic process,
- presence of the catalytical Ni-YSZ SOFC anode,
- fluctuations of the gas composition (according to data presented in Table 2).

The dynamic changes in fuel composition shifted the operating conditions beyond the carbon deposition boundary in some parts of the conducted experiment. The results indicate that fuels with carbon-rich compounds are more demanding in system tests and that thermodynamic calculations should definitely take into account their variations as well as the presence of a catalytic anodic surface. In such system design additional steps need to be taken, like further humidification ($S:C > 2.2$) of fuel in order to extend the safe zone for possible fluctuations in gas composition or operation at higher temperatures.

Figure 17 demonstrates the traces of mechanical contact between the steel interconnect and the anode. The visible carbon particles deposited mainly at the inlet of the fuel electrode in areas which were open for flow, between the contact lines.

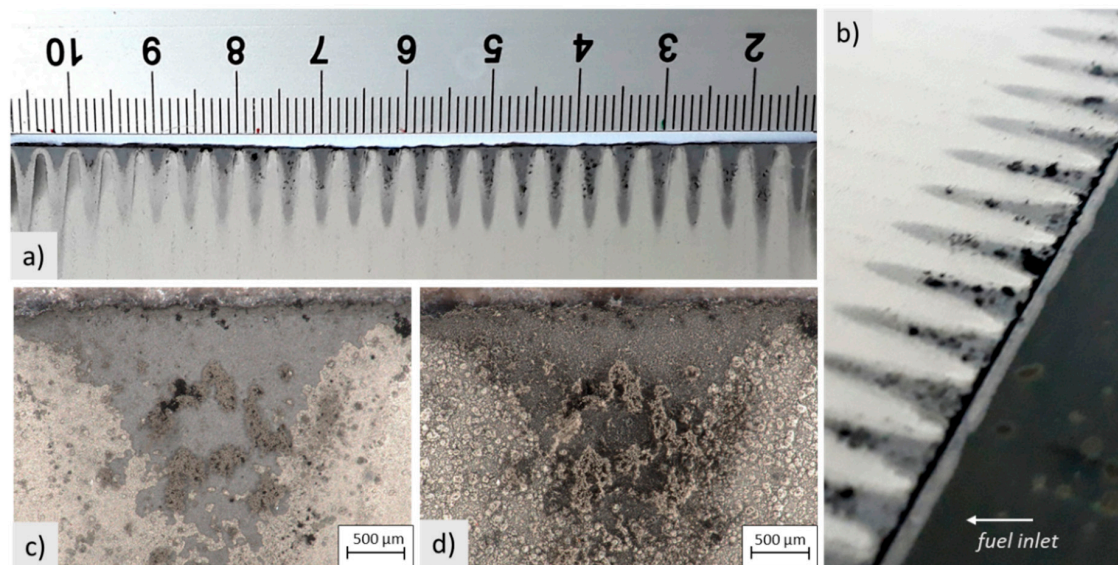


Figure 17. The view of the edge of the fuel cell's anode side (anode support), adjacent to the fuel inlet, after disassembly of the AS-SOFC stack. (a) Extracted from the sealed compartment (flat view), (b) sealed to the metallic compartment of the stack (side view), (c) microscopic observation of the exemplary deposit on the anode (no filter), and (d) microscopic observation of the exemplary deposit on the anode (with spatial filter).

The observations of the deposits and the nearby surface were carried out with a Keyence VHS7000 digital microscope, in order to analyze the nature of the visible spots. The images presented in Figure 17c,d show the damage to the nickel contact layer (the outermost layer). The image obtained with no filter (Figure 17c) does not provide a direct answer as to its nature, with a spatial filter and observation from different angles (Figure 17d) it was confirmed that the outer layer was damaged approximately 100 μm deep inside. Some of the deposits were loose, not connected with the surface, and easy to remove from it, while some of them were joined with the surface. The thickness of the latter varied from ca. 50 to 200 μm .

Scanning electron microscopy investigations with Zeiss Ultra Plus equipment were carried out in order to investigate the anode surface in detail and to find out if the carbon deposits occurred elsewhere. Energy Dispersive X-ray method (EDX) was used to identify the elements occurring on the surface. Figure 18a shows the backscattered electron images of the anode support of Ni-8YSZ after disassembly from the stack (postmortem). The shaded black area is the carbon deposition, which was confirmed by the map generated via Energy Dispersive Spectroscopy (EDS) (Figure 18b).

Analysis of the support surface revealed that the carbon particles were deposited not only in the obvious, observed areas near the edge of the cell adjacent to the fuel inlet, but also all over the anode surface. With the SE detector it was possible to determine the microstructure of such micro-deposits of the amorphous carbon (Figure 18c,d)—they consisted of nanometric particles.

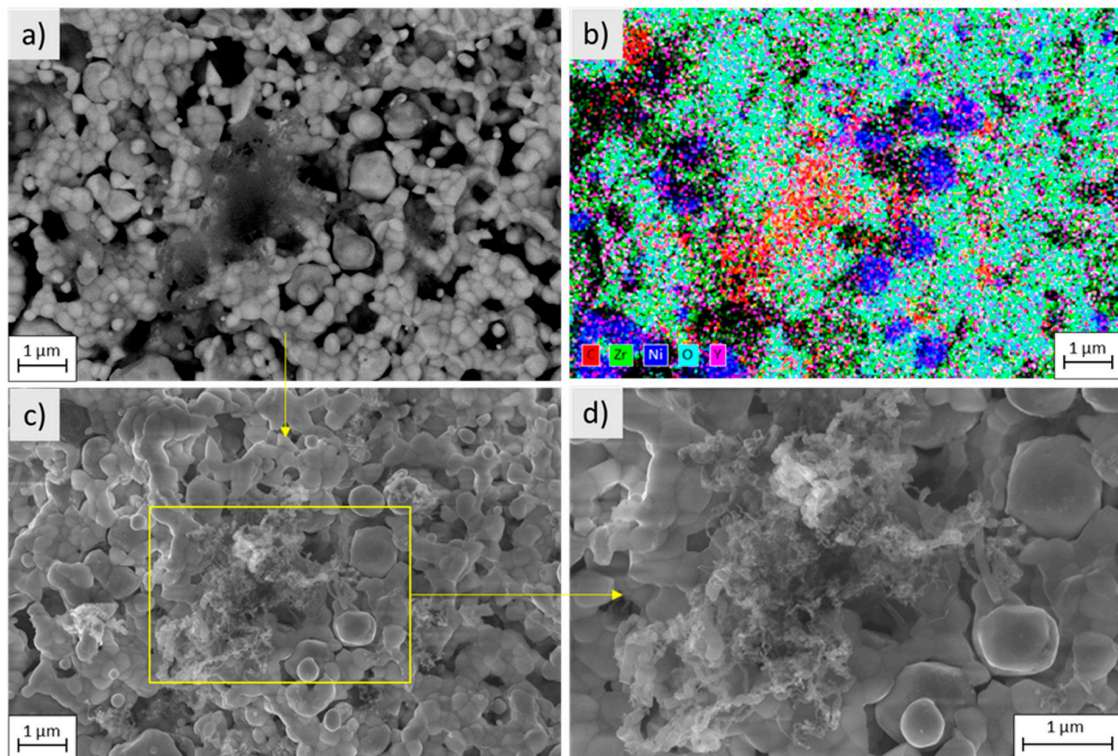


Figure 18. SEM/EDS micrographs from the anode support surface, after disassembly from the stack (postmortem). (a) 25,000 magnification with AsB detector, (b) EDS map of elements, (c) 25,000 magnification with SE2 detector, and (d) 50,000 magnification.

3.3. Comparison of Carbon Contamination for Single-Cell and Stack Environments

As part of this work AS-SOFCs exposed to carbon rich fuel were analyzed in two arrangements: single-cell housing and a 5-cell stack. The single fuel cell was fueled by simulated syngas whereas the AS-SOFC stack was fueled by real syngas produced by the KAJOT two stage gasifier. For the purpose of comparison, tests were performed under constant current load (0.2 A/cm^2) and a similar initial velocity profile (0.3 m/s) in gas channels along the anode surface. Due to limitations in the stack construction and test stand, the tests with single cells and stack were performed at $750 \text{ }^\circ\text{C}$ and $680 \text{ }^\circ\text{C}$, respectively.

The AS-SOFCs applied had a similar anode support composition but differed by thickness and active area. The aim of this approach was to demonstrate similarities in the carbon deposition process despite the geometrical differences between the fuel cells. In the case of a 1-mm-thick single cell, the active area was 16 cm^2 . For the stack analysis, five 0.55 mm thick cells, each with 92 cm^2 of active area, were used. Active areas coincided with the screen-printed cathode area.

In Figure 19, voltage drops were shown with reference to the initial velocity in gas channels of the single fuel cell unit and fuel cell stack. Dots in the chart represent the actual voltage drop measurements, while thin lines are approximations for visualization purposes only. Experimental results of stack's fuel cells demonstrate an intensive degradation process (ca. $1250 \text{ mV}/1000 \text{ h}$) where rapid, transition, and slow degradation zones cannot be distinguished.

In terms of total voltage drop over 80 h, both tests present similarities which can be explained by an analogical amount of deposited carbon within the anode volume. However, except for the total voltage drop, the process character could also be correlated with the different thicknesses of fuel cells. In the case of anode support that was almost half as thin, the carbon deposition was more detrimental although the total anode volume was almost ten times bigger. In contrast to the thick (1 mm) fuel cell, in the SOFC stack, carbon penetrated the whole volume of the fuel electrodes, also reaching triple phase boundaries (TPB) where electrochemical reactions take place. This explains the inability to

separate fast, transition, and slow degradation processes. In the first stage of single fuel cell testing, carbon deposited mainly on the gas–anode interface (fast degradation). With time it started to penetrate inside the anode (transition zone) until it reached the TPB (slow degradation).

To sum up, the realized experiments revealed a correlation between the thickness of the fuel cells and their operating parameters on the carbon formation process. Dynamic changes in fuel composition shifted the operating conditions to more severe than initially planned. An anode of half the thickness could not compensate for such rapid changes. In such a system even short fluctuations in the syngas composition, especially beyond the thermodynamically-safe zone were enough to trigger the carbon deposition process. As a result, the process was very destructive and comparable to one with the single cell, where operating conditions were more detrimental (in terms of thermodynamics) than in the stack environment.

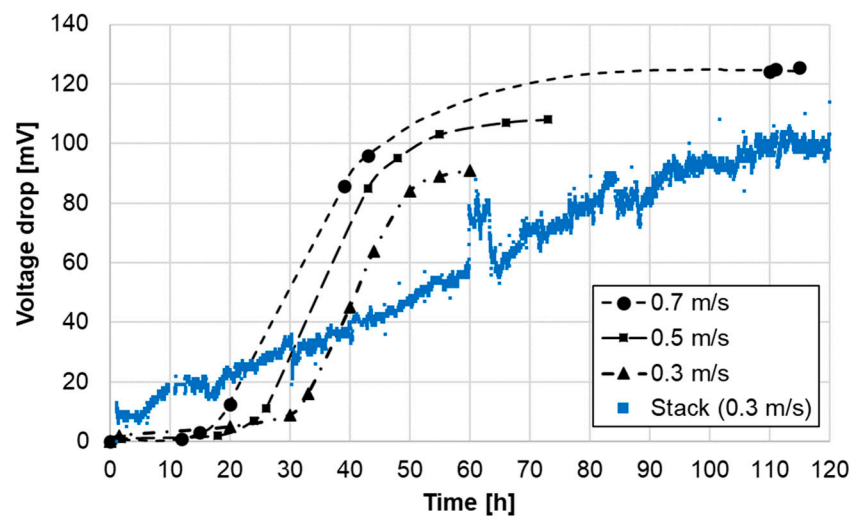


Figure 19. Comparison of voltage drops for single fuel cell and complete stack under constant current load equivalent to current density of 0.2 A/cm^2 recorded at operating temperature of $750 \text{ }^\circ\text{C}$.

4. Summary

The current work was focused on basic research in the field of solid oxide fuel cells, in relation to carbon formation and deposition in the anodic compartments of SOFCs. The findings of the study can be summarized as follows:

1. Higher velocity accelerates the degradation of solid oxide cells in the region which corresponds to irreversible changes (Zone 2).
2. Anode thickness affects performance in such a way that performance of SOFCs with a thin electrode degrades faster than for those with a thick electrode. This is related to carbon deposits located directly in the TPB. As such, thickening the anode can be considered as a countermeasure to inhibit performance degradation due to carbon formation from hydrocarbonaceous fuels.
3. Lowering the operating temperature of an SOFC fed by hydrocarbonaceous fuels favors carbon deposition. This is directly related to the carbon formation isotherms, which were presented using ternary diagrams.
4. Measurements performed in stack conditions included visual inspection of the gas delivery link in order to determine whether carbon deposits were located in the pipes and fittings. No deposits outside the anodic compartments of the SOFC stack were identified. This is related to the catalytic properties of the anodic material.

It is worth mentioning that the statistical quality of data measured in single-cell and 5-cell stack conditions was sufficient to interpret and g such as acceptable level of degradation and expected lifetime.

Thickening of the anode can result in better stability against conditions which favor carbon formation and deposition, lowering degradation, and ultimately boosting SOFC performance and lifetime.

Author Contributions: Conceptualization, K.M., M.S., M.W. and J.K.; Methodology, K.M., M.B. (Marcin Blesznowski), M.S., M.W. and J.K.; Software, K.M.; Validation, K.M., M.B. (Marcin Blesznowski), M.S. and A.Z.; Formal Analysis, K.M. and M.B. (Marcin Blesznowski); Investigation, K.M., M.B. (Marcin Blesznowski), M.S., M.W., A.B. and M.B. (Maciej Bakala); Resources, M.W. and A.B.; Data Curation, K.M., M.S., M.W. and M.B. (Maciej Bakala); Writing-Original Draft Preparation, K.M., M.B. (Marcin Blesznowski), M.S. and J.K.; Writing-Review & Editing, K.M., M.B. (Marcin Blesznowski), M.S., A.Z., M.B. (Maciej Bakala) and J.K.; Visualization, K.M., M.B. (Marcin Blesznowski) and M.S.; Supervision, K.M., M.S. and J.K.; Project Administration, K.M. and M.S.; Funding Acquisition, K.M., M.S. and J.K. All authors have read and agreed to the published version of the manuscript.

Funding: This work was financially supported by the National Science Center, Poland, grant No. 2015/19/N/ST8/01876 and by the Polish National Centre for Research and Development, grant number BIOENERGY-11/BIO-CCHP/2018, for the BIO-CCHP project within the framework of the 11th Joint Call of ERA-NET Bioenergy.

Acknowledgments: The authors would also like to thank Yevgeniy Naumovich for technical and scientific support which enhanced the quality of performed analysis and the numerical and experimental campaign.

Conflicts of Interest: The authors declare no conflict of interest.

References

1. Liso, V.; Zhao, Y.; Brandon, N.; Nielsen, M.P.; Kær, S.K. Analysis of the impact of heat-to-power ratio for a SOFC-based mCHP system for residential application under different climate regions in Europe. *Int. J. Hydrog. Energy* **2011**, *36*, 13715–13726. [[CrossRef](#)]
2. Powell, M.R.; Meinhardt, K.D.; Sprenkle, V.; Chick, L.; McVay, G. Demonstration of a highly efficient solid oxide fuel cell power system using adiabatic steam reforming and anode gas recirculation. *J. Power Sources* **2012**, *205*, 377–384. [[CrossRef](#)]
3. Beigzadeh, M.; Pourfayaz, F.; Ahmadi, M.H. Modeling and improvement of solid oxide fuel cell-single effect absorption chiller hybrid system by using nanofluids as heat transporters. *Appl. Therm. Eng.* **2020**, *166*, 114707. [[CrossRef](#)]
4. Santarelli, M.; Briesemeister, L.; Gandiglio, M.; Herrmann, S.; Kuczynski, P.; Kupecki, J.; Lanzini, A.; Llovel, F.; Papurello, D.; Spliethoff, H.; et al. Carbon recovery and re-utilization (CRR) from the exhaust of a solid oxide fuel cell (SOFC): Analysis through a proof-of-concept. *J. CO₂ Util.* **2017**, *18*, 206–221. [[CrossRef](#)]
5. Kupecki, J.; Jewulski, J.; Motylinski, K. Parametric evaluation of a micro-CHP unit with solid oxide fuel cells integrated with oxygen transport membranes. *Int. J. Hydrog. Energy* **2015**, *40*, 11633–11640. [[CrossRef](#)]
6. Ramadhani, F.; Hussain, M.A.; Mokhlis, H.; Hajimolana, S. Optimization strategies for Solid Oxide Fuel Cell (SOFC) application: A literature survey. *Renew. Sustain. Energy Rev.* **2017**, *76*, 460–484. [[CrossRef](#)]
7. Singhal, S.C.; Kendall, K. *High Temperature Solid Oxide Fuel Cells: Fundamentals, Design and Applications*; Elsevier: Amsterdam, The Netherlands, 2003.
8. Srinivasan, S. *Fuel Cells. From Fundamentals to Applications*; Springer: Berlin/Heidelberg, Germany, 2006.
9. Song, C. Fuel processing for low-temperature and high-temperature fuel cells. Challenges, and opportunities for sustainable development in the 21st century. *Catal. Today* **2002**, *77*, 17–49. [[CrossRef](#)]
10. Kupecki, J.; Skrzyplikiewicz, M.; Wierzbiński, M.; Stepien, M. Analysis of a micro-CHP unit with in-series SOFC stacks fed by biogas. *Energy Procedia* **2015**, *75*, 2021–2026. [[CrossRef](#)]
11. Rokn, M. Thermodynamic analyses of municipal solid waste gasification plant integrated with solid oxide fuel cell and Stirling hybrid system. *Int. J. Hydrog. Energy* **2015**, *40*, 7855–7869. [[CrossRef](#)]
12. Lanzini, A.; Madi, H.; Chiodo, V.; Papurello, D.; Maisano, S.; Santarelli, M.; Van Herle, J. Dealing with fuel contaminants in biogas-fed solid oxide fuel cell (SOFC) and molten carbonate fuel cell (MCFC) plants: Degradation of catalytic and electro-catalytic active surfaces and related gas purification methods. *Prog. Energy Comb. Sci.* **2017**, *61*, 150–188. [[CrossRef](#)]
13. Papurello, D.; Lanzini, A.; Tognana, L.; Silvestri, S.; Santarelli, M. Waste to energy: Exploitation of biogas from organic waste in a 500 W solid oxide fuel cell (SOFC) stack. *Energy* **2015**, *85*, 145–158. [[CrossRef](#)]

14. Kupecki, J.; Skrzypkiewicz, M.; Wierzbicki, M.; Stepien, M. Experimental and numerical analysis of a serial connection of two SOFC stacks in a micro-CHP system fed by biogas. *Int. J. Hydrog. Energy* **2017**, *42*, 3487–3497. [[CrossRef](#)]
15. Kupecki, J.; Jewulski, J.; Badyda, K. Comparative study of biogas and DME fed micro-CHP system with solid oxide fuel cell. *Appl. Mech. Mater.* **2012**, *267*, 53–56. [[CrossRef](#)]
16. Meng, X.; De Jong, W.; Pal, R.; Verkooijen, A.H. In bed and downstream hot gas desulphurization during solid fuel gasification: A review. *Fuel Process. Technol.* **2010**, *91*, 964–981. [[CrossRef](#)]
17. Błesznowski, M.; Jewulski, J.; Zieleniak, A. Determination of H₂S and HCl concentration limits in the fuel for anode supported SOFC operation. *Cent. Eur. J. Chem.* **2013**, *11*, 960–967. [[CrossRef](#)]
18. Van Biert, L.; Visser, K.; Aravind, P.V. A comparison of steam reforming concepts in solid oxide fuel cell systems. *Appl. Energy* **2020**, *264*, 114748. [[CrossRef](#)]
19. Thattai, A.T.; van Biert, L.; Aravind, P.V. On direct internal methane steam reforming kinetics in operating solid oxide fuel cells with nickel-ceria anodes. *J. Power Sources* **2017**, *370*, 71–86. [[CrossRef](#)]
20. Barelli, L.; Bidini, G.; Cinti, G. Steam vs. Dry Reformer: Experimental Study on a Solid Oxide Fuel Cell Short Stack. *Catalysts* **2018**, *8*, 599. [[CrossRef](#)]
21. Hagen, A. Sulfur Poisoning of the Water Gas Shift Reaction on Anode Supported Solid Oxide Fuel Cells. *J. Electrochem. Soc.* **2012**, *160*, 111–118. [[CrossRef](#)]
22. Li, C.; Shi, Y.; Cai, N. Carbon deposition on nickel cermet anodes of solid oxide fuel cells operating on carbon monoxide fuel. *J. Power Sources* **2013**, *225*, 1–8. [[CrossRef](#)]
23. Alzate-Restrepo, V.; Hill, J.M. Carbon deposition on Ni/YSZ anodes exposed to CO/H₂ feeds. *J. Power Sources* **2010**, *195*, 134451. [[CrossRef](#)]
24. PENCHINI, D.; CINTI, G.; DISCEPOLI, G.; SISANI, E.; DESIDERI, U. Characterization of a 100 W SOFC stack fed by carbon monoxide rich fuels. *Int. J. Hydrog. Energy* **2013**, *38*, 525–531. [[CrossRef](#)]
25. Gholaminezhad, I.; Paydar, M.H.; Jafarpur, K.; Paydar, S. Multi-scale mathematical modeling of methane-fueled SOFCs: Predicting limiting current density using a modified Fick's model. *Energy Convers. Manag.* **2017**, *148*, 222–237. [[CrossRef](#)]
26. Kupecki, J. Modeling platform for a micro-CHP system with SOFC operating under load changes. *Appl. Mech. Mater.* **2014**, *607*, 205–208. [[CrossRef](#)]
27. Badyda, K.; Kupecki, J.; Milewski, J. Modelling of integrated gasification hybrid power systems. *Rynek Energii* **2010**, *88*, 74–79.
28. Kupecki, J.; Jewulski, J.; Badyda, K. Selection of a fuel processing method for SOFC-based micro-CHP system. *Rynek Energii* **2011**, *97*, 157–162.
29. Subotic, V.; Schluckner, C.; Stoeckl, B.; Reichholf, D.; Lawlor, V.; Pofahl, S.; Schroettner, H.; Hochenauer, C. In-Operando Detection of Carbon Depositions and Carbon Formation Predictions for Industrial-Sized SOFCs Fueled with Synthetic Diesel Reformate. *ECS Trans.* **2017**, *78*, 2451–2460. [[CrossRef](#)]
30. Jaworski, Z.; Zakrzewska, B.; Pianko-Oprych, P. On thermodynamic equilibrium of carbon deposition from gaseous C-H-O mixtures: Updating for nanotubes. *Rev. Chem. Eng.* **2016**, *33*, 217–235. [[CrossRef](#)]
31. Khan, M.S.; Lee, S.-B.; Song, R.-H.; Lee, J.-W.; Lim, T.-H.; Park, S.-J. Fundamental mechanisms involved in the degradation of nickel-yttria stabilized zirconia (Ni-YSZ) anode during solid oxide fuel cells operation: A review. *Ceram. Int.* **2016**, *42*, 35–48. [[CrossRef](#)]
32. Lanzini, A.; Leone, P.; Guerra, C.; Smeacetto, F.; Brandon, N.; Santarelli, M. Durability of anode supported Solid Oxides Fuel Cells (SOFC) under direct dry reforming of methane. *Chem. Eng. J.* **2013**, *220*, 254–263. [[CrossRef](#)]
33. Stoeckl, B.; Subotić, V.; Preininger, M.; Schroettner, H.; Hochenauer, C. SOFC operation with carbon oxides: Experimental analysis of performance and degradation. *Electrochim. Acta* **2018**, *275*, 256–264. [[CrossRef](#)]
34. Chen, T.; Wang, W.G.; Miao, H.; Li, T.; Xu, C. Evaluation of carbon deposition behavior on the nickel/yttrium-stabilized zirconia anode-supported fuel cell fueled with simulated syngas. *J. Power Sources* **2011**, *196*, 2461–2468. [[CrossRef](#)]
35. Koh, J.H.; Yoo, Y.S.; Park, J.W.; Lim, H.C. Carbon deposition and cell performance of Ni-YSZ anode support SOFC with methane fuel. *Solid State Ion.* **2002**, *149*, 157–166. [[CrossRef](#)]
36. Lyu, Z.; Li, H.; Han, M. Electrochemical properties and thermal neutral state of solid oxide fuel cells with direct internal reforming of methane. *Int. J. Hydrog. Energy* **2019**, *44*, 12151–12162. [[CrossRef](#)]

37. Silva-Mosqueda, D.M.; Elizalde-Blancas, F.; Pumiglia, D.; Santoni, F.; Boigues-Muñoz, C.; McPhail, S.J. Intermediate temperature solid oxide fuel cell under internal reforming: Critical operating conditions, associated problems and their impact on the performance. *Appl. Energy* **2019**, *235*, 625–640. [[CrossRef](#)]
38. Papurello, D.; Iafrate, C.; Lanzini, A.; Santarelli, M. Trace compounds impact on SOFC performance: Experimental and modelling approach. *Appl. Energy* **2017**, *208*, 637–654. [[CrossRef](#)]
39. Takeguchi, T.; Kikuchi, R.; Yano, T.; Eguchi, K.; Murata, K. Effect of precious metal addition to Ni-YSZ cermet on reforming of CH₄ and electrochemical activity as SOFC anode. *Catal. Today* **2003**, *84*, 217–222. [[CrossRef](#)]
40. Takeguchi, T.; Kani, Y.; Yano, T.; Kikuchi, R.; Eguchi, K.; Tsujimoto, K.; Uchida, Y.; Ueno, A.; Omoshiki, K.; Aizawa, M. Study on steam reforming of CH₄ and C₂ hydrocarbons and carbon deposition on Ni-YSZ cermets. *J. Power Sources* **2002**, *112*, 588–595. [[CrossRef](#)]
41. Borowiecki, T.; Gotebiowski, A.; Stasifiska, B. Effects of small MoO₃ additions on the properties of nickel catalysts for the steam reforming of hydrocarbons. *Appl. Catal. A Gen.* **1997**, *153*, 141–156. [[CrossRef](#)]
42. Niakolas, D.K.; Ouweltjes, J.; Rietveld, G.; Dracopoulos, V.; Neophytides, S.G. Au-doped Ni/GDC as a new anode for SOFCs operating under rich CH₄ internal steam reforming. *Int. J. Hydrog. Energy* **2010**, *35*, 7898–7904. [[CrossRef](#)]
43. Skrzypkiewicz, M.; Jewulski, J.; Lubarska-Radziejewska, I. The effect of Fe₂O₃ catalyst on direct carbon fuel cell performance. *Int. J. Hydrog. Energy* **2015**, *40*, 13090–13098. [[CrossRef](#)]
44. Niakolas, D.K.; Ouweltjes, J.; Rietveld, G.; Dracopoulos, V.; Neophytides, S.G. Near net shape manufacturing of planar anode supported solid oxide fuel cells by using ceramic injection molding and screen printing. *J. Power Sources* **2014**, *268*, 752–757. [[CrossRef](#)]
45. Niakolas, D.K.; Ouweltjes, J.; Rietveld, G.; Dracopoulos, V.; Neophytides, S.G. Characterization of a circular 80 mm anode supported solid oxide fuel cell (AS-SOFC) with anode support produced using high-pressure injection molding (HPIM). *Int. J. Hydrog. Energy* **2019**, *44*, 19405–19411. [[CrossRef](#)]
46. Subotić, V.; Baldinelli, A.; Barelli, L.; Scharler, R.; Pongratz, G.; Hochenauer, C.; Anca-Couce, A. Applicability of the SOFC technology for coupling with biomass-gasifier systems: Short- and long-term experimental study on SOFC performance and degradation behaviour. *Appl. Energy* **2019**, *256*, 113904. [[CrossRef](#)]
47. Golec, T. *Energetyczne Wykorzystanie Biomasy Poprzez Spalanie i Zgazowanie*; Wydawnictwo Naukowe Instytutu Technologii Eksploatacji—PIB, Institute of Power Engineering—Research Institute: Warsaw, Poland, 2014.
48. Singh, D.; Hernández-Pacheco, E.; Hutton, P.N.; Patel, N.; Mann, M.D. Carbon deposition in an SOFC fuelled by tar-laden biomass gas: A thermodynamic analysis. *J. Power Sources* **2005**, *142*, 194–199. [[CrossRef](#)]
49. Bebelis, S.; Neophytides, S. AC impedance study of Ni-YSZ cermet anodes in methane-fuelled internal reforming YSZ fuel cells. *Solid State Ion.* **2002**, *152–153*, 447–453. [[CrossRef](#)]
50. Subotić, V.; Menzler, N.H.; Lawlor, V.; Fang, Q.; Pofahl, S.; Harter, P.; Schroettner, H.; Hochenauer, C. On the origin of degradation in fuel cells and its fast identification by applying unconventional online-monitoring tools. *Appl. Energy* **2020**, *277*, 115603. [[CrossRef](#)]

Publisher’s Note: MDPI stays neutral with regard to jurisdictional claims in published maps and institutional affiliations.



© 2020 by the authors. Licensee MDPI, Basel, Switzerland. This article is an open access article distributed under the terms and conditions of the Creative Commons Attribution (CC BY) license (<http://creativecommons.org/licenses/by/4.0/>).